Journal of Photochemistry and Photobiology A: Chemistry 222 (2011) 25–33

Contents lists available at ScienceDirect

Journal of Photochemistry and Photobiology A: Chemistry

journal homepage: www.elsevier.com/locate/jphotochem

Photo-induced formation of size-selective Ag nanoparticles and their interactions with *Escherichia coli*

Subrata Kundu*, Hong Liang

Materials Science and Mechanical Engineering, Texas A&M University, College Station, TX 77843-3123, USA

ARTICLE INFO

Article history:
Received 6 January 2011
Received in revised form 15 March 2011
Accepted 27 March 2011
Available online 13 June 2011

Keywords:
ATP
Ag NPs
CTAB
UV-irradiation
Escherichia coli

ABSTRACT

A new synthetic route was utilized for the formation of size-selective Ag nanoparticles (NPs) exploiting UV-irradiation techniques. The one step process exclusively generates Ag NPs of smaller sizes, larger sizes and aggregated nanostructures. The reduction of Ag(I) was done in the presence of adenosine tri-phosphate (ATP) under 30 min of UV-irradiation. ATP served as a dual role, a reducing agent and a stabilizing agent for the formation of Ag NPs. The mechanisms of the particle formation and the effects of different reaction parameters were studied in details. The synthesized particles were stable for more than a month under ambient condition without indication of oxide formation. Moreover, the method did not need any harsh reduction conditions. The synthesized negatively charged ATP–Ag NPs has been mixed with bacteria *Escherichia coli* and studied their interaction. Finally a comparative study was made with the ATP–Ag NPs with positively charged CTAB–Ag NPs. The results indicated that positively charged Ag NPs deposited better with the bacterium surface compared to the negatively charged. The present research might find important applications for the synthesis of other nanomaterials as well as to understand the interactions of NPs with microorganisms.

1. Introduction

In recent years, synthesis and characterization of colloidal metal particles in the 'neglected dimension' have shown tremendous importance due to their promising application in chemistry, biology, physics, materials science, medicine, and electronics. Metal nanoparticles exhibit special properties when compared to their bulk element. This is possible because of their high surface-to-volume ratio and unique optical [1], electronic [2], magnetic [3] and catalytic [4] properties. Most of these properties are strongly depend upon the size and shape of the particles as well as the surrounding medium. Among the different colloidal metal nanoparticles (NPs), novel metal NPs have shown particular interest due to their close lying valence and conduction bands in which the electron moves freely. As the properties of novel metallic nanoparticles change with their size and shape, an effective route is required for synthesis of NPs with control of the same. Among the various synthetic routes, chemical synthesis methods are superior to physical methods for controlling the size and shapes.

It is proven that Ag NPs are superior to other metals due to their high electric conductivity [5], optical properties [6], antimicrobial effect [7], use as oxidative catalyst [8] and spatial Raman spectroscopic [9] behavior. Moreover, Ag NPs have strong surface plasmon resonance (SPR) band in the visible region and that helps the study of the evolution and characterization of the particles in solution. In the literature there are a number of chemical methods reported for the synthesis of Ag NPs [10–16]. The easiest and well-known method is the reduction of silver ions in the presence of $NaBH_4$ or tri-sodium citrate to obtain negatively charged Ag NPs [10,11]. Several other methods include polyol process [12], γ-radiolytic process [13], sonochemical process [14], laser irradiation techniques [15] and microwave heating [16]. Liu et al. synthesized size-selective Ag NPs in poly-vinyl-pyrrolidone solution in the presence of metallic seed particles [17]. Tan et al. synthesized Ag NPs by the reduction of Ag salt using potassium bi-tartrate as a reducing agent and stabilized the particles in a polymeric solution [18]. Kundu et al. synthesized Ag nanocubes using microwave heating method for a very short time in poly (styrene) sulfonate (PSS) solution [19]. A photochemical method was used for the synthesis of SERS (surface enhanced Raman scattering) active Ag NPs in silica matrix [20]. Gedanken's group synthesized Ag NPs on silica spheres using a sonochemical deposition method [21]. Recently, our group synthesized Ag NPs in a non-ionic surfactant media using alkaline 2,7-dihydroxy naphthalene (2,7-DHN) as reducing agent under microwave irradiation techniques [16]. Most of the above methods were either time consuming, needing multiple steps for

* Corresponding author. Current address: Electrochemical Materials Science (ECMS) Division, Central Electrochemical Research Institute (Council of Scientific and Industrial Research), Karaikudi - 630 006, Tamil Nadu, India.
Tel.: +91 4565 227550 559x264/224; fax: +91 4565 227779/227713.
E-mail addresses: subrata_kundu2004@yahoo.co.in (S. Kundu), hliang@tamu.edu (H. Liang).

1010-6030/$ – see front matter © 2011 Elsevier B.V. All rights reserved.
doi:10.1016/j.jphotochem.2011.03.024

Table 1
Details concentrations, size of the particles, UV-irradiation time for the formation of ATP stabilized Ag NPs.

Set number	Final conc. of ATP solution (M)	Final conc. of $AgNO_3$ solution (M)	Time of UV-irradiation (min)	Color of the final product	Shape of the particles	Diameter of the particles (nm)
1	9.09×10^{-2}	9.09×10^{-3}	30	Yellowish	Spherical	$\sim 3.5 \pm 1.5$
2	9.09×10^{-2}	9.09×10^{-4}	30	Light orange	Spherical	$\sim 37 \pm 0.5$
3	9.09×10^{-3}	9.09×10^{-4}	30	Dark orange	Honey comb like aggregated	$\sim 12 \pm 0.5$

the synthesis, or generated various shapes with uncontrollable size distributions.

Recently, different biological molecules like proteins [22], peptides [23], amino acids [24] and DNA (deoxyribo-nucleic acid) [25] have been used for the synthesis and fabrication of metal NPs. The nucleic acid or nucleotide mediated synthesis of metal NPs is an emerging area. The major advantage of nucleotide mediated synthesis is that the size and the chemical property of the NPs can be tuned according to the structure of the nucleic acid. The other advantages are, (a) they can bind with different metal ions via different well established binding modes, (b) nucleic acid in solution provide well defined 3-D shape which can be used for molecular building blocks like squares [26], cubes [27], T-junctions [28], etc., (c) nucleic acid sequences are much more cost-effective than polypeptide sequences. Kelley and Eaton reported earlier that the chemical properties of the NPs could be changed according to the constituent nucleotide or nucleotide tri-phosphate building blocks [29,30]. Recently, we synthesized metal [31] and semi-conductor [2] nanowires using DNA as template either using microwave heating or UV-irradiation method. Adenine coated Ag NPs were synthesized by Wei et al. by the reduction of Ag ions in $NaBH_4$ solution [32]. In the present work, we use UV-irradiation to synthesize Ag NPs using adenosine-tri-phosphate (ATP) as a stabilizing and reducing agent.

Here, we report the size-selective synthesis of Ag NPs using a simple photochemical approach. The reduction of Ag(I) ions was done in the presence of ATP under 30 min of continuous UV-irradiation. ATP acted as a reducing agent during the synthesis as well as a stabilizing agent after the formation of the NPs. The method produced various sized and aggregated Ag NPs via tuning the metal ion-to-ATP-molar ratio. The synthesized Ag NPs were deposited on the bacterium *Escherichia coli* (*E. coli*) to study their interactions. Moreover, positively charged CTAB (cetyl trimethylammonium bromide) stabilized Ag NPs were also synthesized and deposited on the bacteria. Finally a comparative study was conducted. It was found that positively charged Ag NPs (CTAB stabilized) interacted better with the bacteria surface compared to the negatively charged (ATP stabilized) Ag NPs. To the best of our knowledge, the synthesis of size-selective Ag NPs using ATP under UV-irradiation and their interactions with bacteria *E. coli* have not been reported before. The present synthesis processes as well as the interactions study with bacteria are simple, straightforward, reproducible, and cost effective.

2. Experimental

2.1. Reagents

Adenosine tri-phosphate (ATP), silver nitrate (99%), and cetyl trimethyl ammonium bromide (CTAB, 99%) were purchased from Sigma–Aldrich and used without further purification. Sodium borohydride ($NaBH_4$) was also purchased from Sigma–Aldrich. The de-ionized (DI) water was used for the entire synthesis process as well as in the NPs–bacteria interaction study.

2.2. Instruments

UV–visible (UV–vis) absorption spectra were recorded in a Hitachi (model U-4100) UV-VIS-NIR spectrophotometer equipped with a 1 cm quartz cuvette holder for liquid samples. A high-resolution transmission electron microscope (HR-TEM) (JEOL JEM 2010) was used at an accelerating voltage of 200 kV. The energy dispersive X-ray spectrum (EDS) was recorded with an Oxford Instruments INCA energy system connected with the TEM. The XRD analysis was done with a scanning rate of 0.020 S^{-1} in the 2θ range 35–85° using a Bruker-AXS D8 Advanced Bragg-Brentano X-ray Powder Diffractometer with Cu Kα radiation ($\lambda = 0.154178$). The X-ray photoelectron spectroscopy (XPS) analysis was carried out using a Kratos Axis Ultra Imaging X-ray photoelectron spectrometer with monochromatic Al Kα line (1486.7 eV). The instrument integrates a magnetic immersion lens and charge neutralization system with a spherical mirror analyzer, which provides real-time chemical state and elemental imaging using a full range of pass energies. The emitted photoelectrons were detected by the analyzer at a passing energy of 20 eV with energy resolution of 0.1 eV. The incident X-ray beam was normal to the sample surface and the detector was 45° away from the incident direction. The analysis spot on the sample was 0.4 mm by 0.7 mm. A xenon lamp from Newport Corporation at a wavelength of 260 nm on the sample was used for UV-photoirradiation. The approximate intensity was 20 ± 0.5 μW and the bandwidth of irradiation was 260 ± 8 nm. The distance of the sample from the light source was 15 cm. The sample was placed over a wooden box with a stand to make the light shine on it directly.

2.3. Size-selective synthesis of ATP stabilized Ag NPs

Size-selective Ag NPs were synthesized by varying the concentrations of $AgNO_3$ with the concentrations of aqueous ATP solution. The solution mixture containing ATP and $AgNO_3$ are mixed well with a magnetic stirrer and then placed under UV-irradiation for about 30 min. For a typical synthesis, 6 mL of 0.1 (M) ATP solution was mixed with 0.6 mL of 0.1 (M) $AgNO_3$ solution and the solution mixture was UV-irradiated for 30 min. The formation of silver particles started within 5 min of UV-irradiation as light yellowish color is observed in the solution mixture. Finally after 30 min of UV-irradiation the color changed to deep reddish yellow. This solution contains spherical Ag NPs with smaller sizes. For other two sizes like larger spheres and aggregated Ag particles we varied the concentration of $AgNO_3$ and ATP keeping the UV-irradiation time fixed for 30 min. The details concentrations, size of the particles, UV-irradiation time is given in Table 1. The colors of the synthesized Ag NPs were stable for more than a month in the dark under ambient condition without change in any optical properties.

2.4. Synthesis of CTAB-stabilized Ag NPs

Positively charged CTAB stabilized Ag NPs are synthesized according to the previous report by Yonezawa et al. [33]. In the synthesis we mixed 10 mL of 5×10^{-3} (M) $AgNO_3$ with 50 mL of 10^{-2} (M) CTAB solution and stirred well. Initially, after mixing the

mixed solution shows white turbidity due to the formation of AgBr. Finally, 5 mL of 0.4 (M) ice-cold $NaBH_4$ solution was added drop wise while stirring vigorously. Stirring was continued another 15–20 min after complete mixing of $NaBH_4$. The solution color changed to dark yellow confirmed the formation of Ag NPs and the solution was stable for more than a week in ambient condition.

2.5. Preparation of sample for UV–vis, TEM, EDS, XRD, and XPS analysis

The Ag NPs were characterized using UV–vis, TEM, EDS, XRD, and XPS measurements. The Ag NPs solution after successive centrifugation was re-dispersed in DI water and used for the measurement in UV-vis spectrophotometer. The samples for TEM and EDS were prepared by placing a drop of the corresponding Ag NP solution onto a carbon-coated Cu grid followed by slow evaporation of solvent at ambient condition. For XRD and XPS analysis, silicon (Si) wafers were used as the substrates for the thin film preparation. The wafers were cleaned thoroughly in acetone and sonicated for about 20 min. The cleaned substrates were covered with the Ag NP solution and dried in a vacuum chamber. After the first layer was deposited, subsequent layers were deposited by repeatedly adding more Ag NP solution and drying. Final samples were obtained after 8–10 depositions and then analyzed using XRD and XPS techniques.

2.6. Preparation of bacteria samples and their incubation with Ag NPs

Bacteria, *E. coli* strain DH5α was used in our current research. These bacteria strains were generously collected from the department of Biology at the Texas A&M University. The *E. coli* was grown in the liquid LB (Luria–Bertani) media at 37 °C and stirred at 250 rpm for overnight (~16 h). After completely grown, the bacteria solution containing *E. coli* was taken in a small centrifuge tube and varied amounts of Ag NPs (both ATP and CTAB stabilized) mixed separately. The mixed solution containing Ag NPs and bacteria was incubated for different times and then spotted over a TEM Cu grid for analysis. The bacteria Ag NPs after spotting on TEM grid were air-dried overnight and then analyzed using TEM and EDS. The detailed results are given in later part of Section 3.

3. Results and discussion

3.1. UV–vis spectroscopy study

Monodispersed Ag NPs with different sizes were synthesized by the reduction of $AgNO_3$ with ATP under 30 min of UV-irradiation. ATP not only acted as a stabilizing agent but also as a reducing agent for the reduction of Ag(I) to Ag(0). ATP directed the growth of Ag NPs and produced different sizes. The ATP is a multifunctional nucleotide generally used in cells as a co-enzyme. One molecule of ATP consists of a three phosphate group which is attached with ribose sugar and that sugar binds with adenine base. Fig. 1A shows the chemical structures of nucleoside, nucleoside-monophosphate, nucleoside-diphosphate, and nucleoside-triphosphate. Fig. 2 shows the UV–vis spectrum of the reaction mixture at different stages of the synthesis process. The colorless aqueous solution of $AgNO_3$ has a very small intense peak at ~302 nm in the visible region (curve A, Fig. 2). The aqueous ATP solution has an absorption band at ~258 nm due to the presence of aromatic base molecule (curve B, Fig. 2). The mixing of ATP with $AgNO_3$ (curve C, Fig. 2) resulted a small peak shift as well as a decrease in absorbance value. This was probably due to interactions of ATP with Ag(I) ions. After UV-irradiation for 30 min with the solution containing ATP and $AgNO_3$, a new peak appeared at 418 nm due to the SPR of spherical Ag NPs [10–16,19,20]. The peak

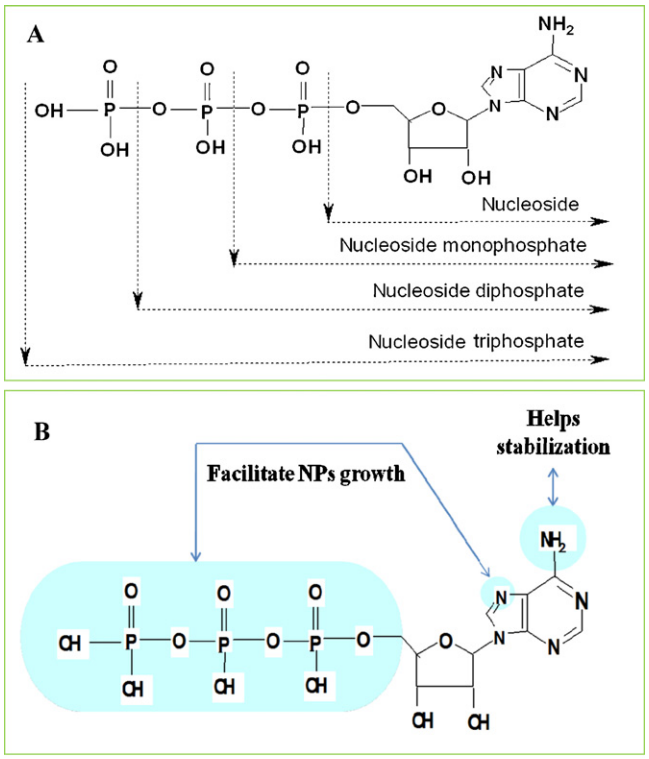

Fig. 1. (A) Chemical structure of the different nucleosides. (B) Schematic representation how the different parts of ATP having different specific roles for Ag-NPs synthesis.

at 418 nm is due to the formation of smaller sized Ag NPs as shown in curve D, Fig. 2. Curves E and F in Fig. 2 shows the SPR bands for larger sizes and aggregated Ag NPs, respectively. With the increase in particles size, the absorption maxima were also shifted towards

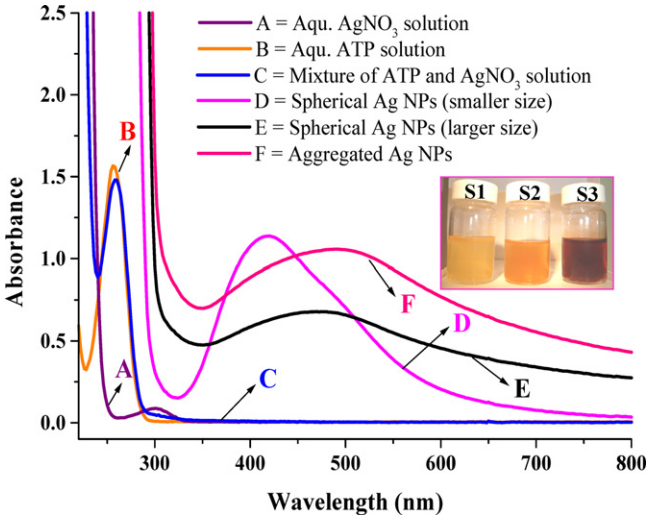

Fig. 2. UV–vis absorption spectra at various stages of ATP–Ag NP synthesis. Curve A shows the absorption spectra of aqueous $AgNO_3$ solution. Curve B shows the absorption spectra of aqueous ATP solution having a band at ~258 nm. Curve C shows the absorption spectra of the mixture of ATP with $AgNO_3$. Curves D, E and F show the surface plasmon resonance (SPR) band for the formation of different sizes Ag NPs. The inset shows three different color images indicated with S1, S2, and S3 containing Ag NPs of different sizes. (For interpretation of the references to color in this figure legend, the reader is referred to the web version of this article.)

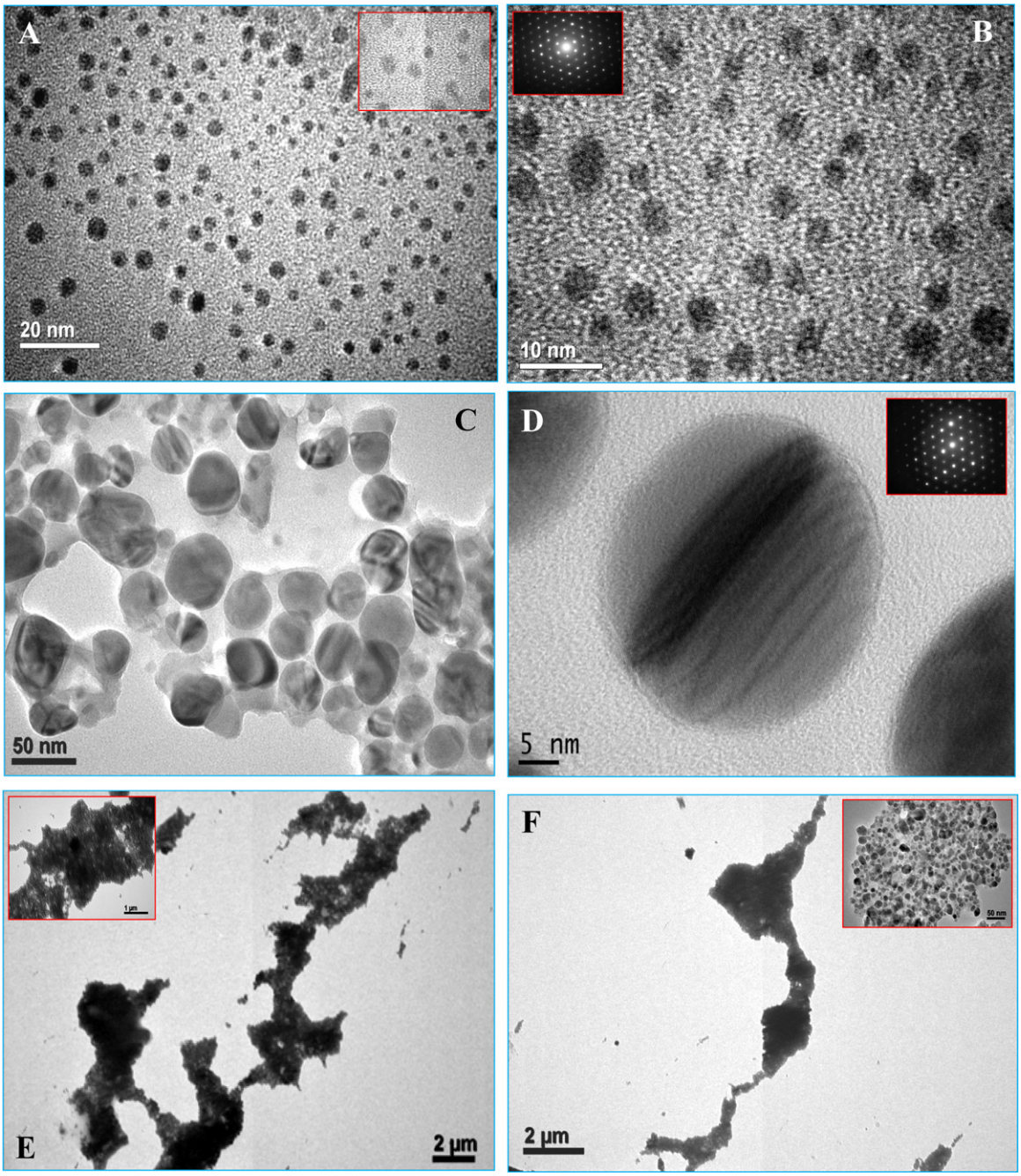

Fig. 3. Transmission electron microscopy (TEM) images for the synthesis of ATP–Ag NPs after 30 min of UV irradiation with variation of reaction conditions. (A and B) Shows the low and high magnified TEM images of spherical Ag NPs having average particles diameter ~3.5 ± 1.5 nm. The inset of (A) shows its corresponding higher magnified image. (C and D) Shows the low and high magnified image of bigger size spherical Ag NPs having average particles sizes ~37 ± 5 nm. The inset of (B and D) shows their corresponding SAED patterns. (E and F) Shows the low magnified images of aggregated Ag NPs and the average lengths are more than 10 μm and the average diameters of a single Ag particle from the aggregates are ~12 ± 5 nm. The inset of (E and F) shows their corresponding higher magnified images.

higher wavelength region which was well matched with the literature report previously. For larger size spherical particles (curve E, Fig. 2), we observed a broad absorption band ranged from 370 to 570 nm with an absorption maxima at 470 nm. Similarly for aggregated Ag NPs (curve F, Fig. 2), we observed a broad peak in the range of 370 and 600 nm with an absorption maxima at 490 nm. The inset of Fig. 2 shows three different color images indicated with S1, S2, and S3 containing Ag NPs of different sizes. S1 signifies the Ag NPs with smaller size, S2 signifies the Ag NPs with larger size, and S3 the aggregated Ag NPs. The synthesized Ag NP solutions were stable for more than a month under dark in the ambient condition.

3.2. Transmission electron microscopy (TEM) analysis

Fig. 3 shows the transmission electron microscopy images of various sized and ATP stabilized Ag NPs. Those were synthesized with the above method (details given in experimental section) after 30 min of UV irradiation. Fig. 3A and B shows the low and high magnified TEM image corresponding to the curve D in Fig. 2. Particles are spherical, separated with an average size of ~3.5 ± 1.5 nm. The inset of Fig. 3A shows its corresponding high magnified image. The inset of Fig. 3B shows the corresponding selected area electron diffraction (SAED) pattern confirming that the ATP stabilized

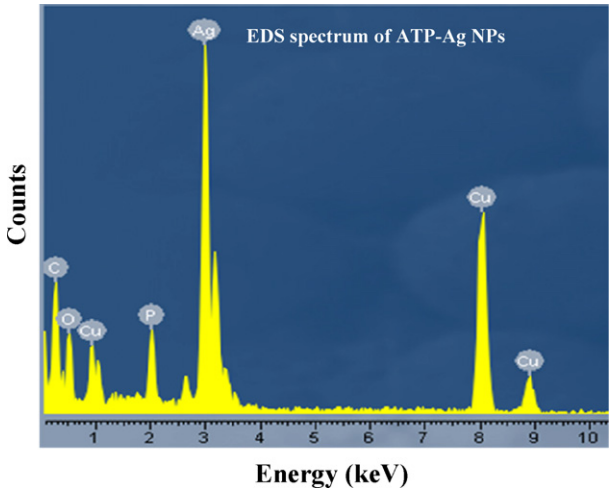

Fig. 4. Energy dispersive X-ray spectrum (EDS) of the ATP–Ag NPs showing the peaks for C, O, Cu, P, and Ag.

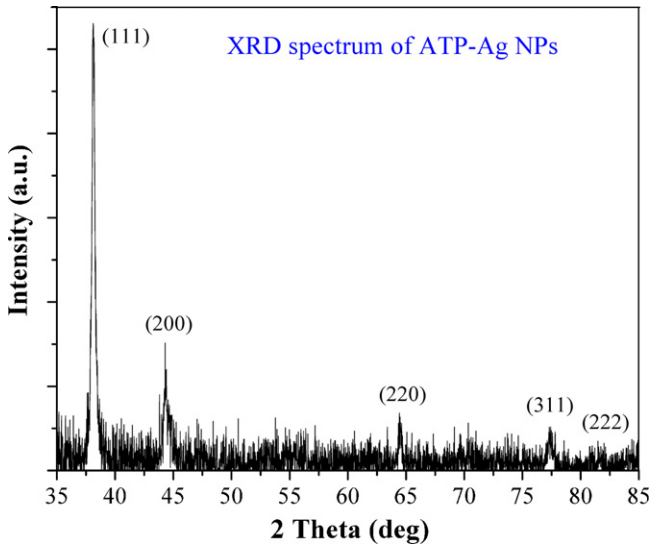

Fig. 5. Powder X-ray diffraction (XRD) pattern of the ATP–Ag NPs having the diffraction from the (1 1 1), (2 0 0), (2 2 0), (3 1 1), and (2 2 2) planes of silver NPs.

Ag NPs are single crystal. Fig. 3C and D shows the low and high magnified images corresponding to curve E in Fig. 2. Here the particles are bigger in size than previous one and the average particles sizes are $\sim 37 \pm 5$ nm. Fig. 3D shows the image of a single particles and the inset shows the corresponding SAED pattern. It confirms that the single crystal nature of the particles. Fig. 3E and F shows the low magnified images of aggregated Ag NPs taken from different parts of the same samples (corresponding to curve F, Fig. 2). From the image it is clear that small Ag NPs aggregated to form the honey-comb like structure. The lengths of the aggregated structures are more than 10 μm. The inset of Fig. 3E and F shows their corresponding high magnified images. From those, it is clear that the average diameters of a single Ag particle from the aggregatesis $\sim 12 \pm 5$ nm. These smaller particles are aggregated together to form the honey comb-like structure. From the above TEM analysis it is clear that different reaction condition produces different sizes Ag NPs.

3.3. Energy dispersive X-ray spectroscopy (EDS) analysis

Fig. 4 shows the results obtained from the energy dispersive X ray spectroscopy (EDS) analysis. EDS analysis is used to determine the elements present in the synthesis. The spectrum consisted of different peaks from the C, O, Cu, P, and Ag. The C and Cu peaks came from the C-coated Cu TEM grid used for the analysis. The P and O peaks came from the ATP used for the synthesis of Ag NPs. The high intense Ag peak came from the Ag NPs. The above EDS result confirms the presence of Ag NPs in the sample.

3.4. X-ray diffraction (XRD) analysis

Fig. 5 shows the powder X-ray diffraction pattern of ATP stabilized Ag NPs. The peaks were assigned to diffraction from the (1 1 1), (2 0 0), (2 2 0), (3 1 1), and (2 2 2) planes of silver NPs (JCPDS card number 4-0783) [24]. These diffraction peaks confirm the presence of a face-centered cubic (fcc) structure of crystalline Ag NPs. The sizes of the Ag NPs were measured by the X-ray diffraction peak's line width using the Debye formula for small crystal spheres. The mean diameters of the Ag particles are consisted with the result from the TEM image. According to the literature, the specific shape of any fcc nano crystal mainly depends by the ratio between growth rates along the <1 0 0> and <1 1 1> directions [34]. Here in our synthesis, we used ATP as a stabilizing agent so the selective interaction between the ATP and different crystal facets of Ag NPs alters the growth rate along the different crystal directions.

3.5. X-ray photoelectron spectroscopy (XPS) analysis

Fig. 6 shows the X-ray photoelectron spectroscopy (XPS) images of a self-assembled Ag NPs film. The sensitivity of XPS in chemical analysis stems mostly from its ability to resolve the chemical identity of the atoms from the measured binding energies. Fig. 6A shows the overall survey and Fig. 6B the Ag (3d) XPS spectra. The survey spectrum consists of the characteristic peaks of O(1s) at 529.5 eV, C(1s) at 282 eV and Ag(3d) peaks. The Ag(3d) region is characterized by a doublet which arises from the spin–orbit coupling (Ag $3d_{5/2}$ and Ag $3d_{3/2}$) as shown in Fig. 6B. The two intense Ag peaks appear at a binding energy of 374.1 (for Ag $3d_{3/2}$) and 368 (for Ag $3d_{5/2}$) eV which clearly indicates the formation of Ag NPs. The peak positions are in agreement with the previous literature [16,35]. In the survey spectrum we did not observe peaks for the oxide formation which indicates the stability of Ag NPs. The O(1s) peak came from the ATP which is bound to the surface of the Ag NPs.

3.6. Effects of other reaction parameters

To standardize the reduction process we examined the variation of reaction parameters like concentration of ATP and Ag(I) ions and the UV-irradiation time. The best result with size selective Ag NPs and aggregated Ag NPs are formed in the concentrations given in the experimental section and in Table 1. We have seen that when Ag(I) concentration is very high ($\geq 10^{-1}$ M), the formation of Ag NPs is very fast (within 5–6 min of UV-irradiation) but particles gets precipitated after few hours of the synthesis. Similarly, when the concentration of Ag(I) is low ($\leq 10^{-4}$ M), the formation of Ag NPs took longer time (>3 h) and formed an un-uniform particles sizes. We also varied the concentrations of ATP and observed that a higher concentration mostly small size spherical particles formed and at lower ATP concentration either bigger or aggregated Ag NPs formed. We also varied the UV-irradiation time and observed that 30 min is sufficient for the formation of size-selective Ag NPs. The Ag NPs started formation within 3–5 min of UV-irradiation and completed after 30 min of UV-irradiation. A long irradiation time (more than 2 h) results the precipitation of the Ag NPs. We tested our reaction with normal conventional heating procedure using

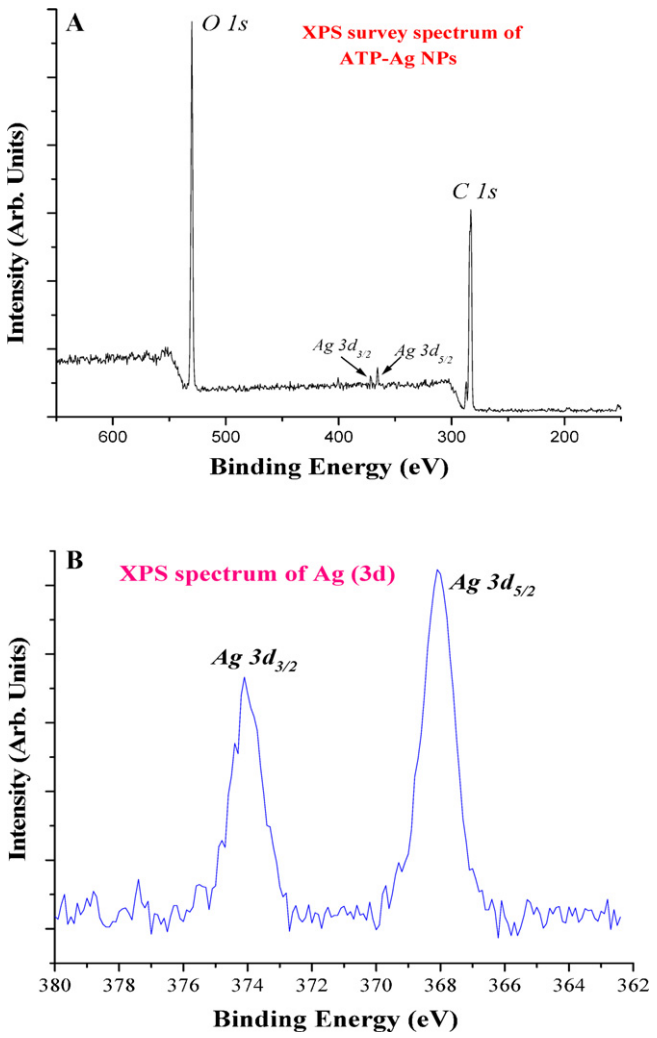

Fig. 6. X-ray photoelectron spectrum (XPS) of the ATP–Ag NPs. (A) is the overall survey spectra and (B) is the spectra for Ag (3d) regions.

conventional heater or using water bath but none of them resulted the formation of Ag NPs in the experimental time scale. Thus all above control experiment proved that the size-selective Ag NPs were formed only at a specific concentration as given in Table 1.

3.7. *Reaction mechanism of Ag NPs formation*

The formation of size-selective Ag NPs was initiated by the reduction of Ag(I) ions in the presence of ATP under UV-photoirradiation. In our proposed synthesis both the presence of ATP and the UV-irradiation is extremely necessary for the formation of Ag NPs. In the absence of ATP, no Ag particles formed due to the absence of reducing agent while in the absence of UV-irradiation no particles formed due to lack of formation of radical species in the solution mixture. So a proper concentration of ATP and a sufficient UV irradiation is necessary for the formation of Ag NPs. Kumar and Mital [36], and Green et al. [37] group reported earlier that nucleosides like ATP, guanosine triphosphate (GTP) acted as a capping agent and templates for the formation of metal and semi-conductor NPs. In their study they used these nucleosides only for capping of templating agents but they did not reveal their reducing property. This nucleotide or nucleic acid based NPs synthesis is a new approach because one could tune the NPs size and their physico-chemical property according to the nucleic acid structure and their compositions. Earlier Kelley [29] and Eaton [30] group reported earlier that properties of NPs could be tuned according to the constituent RNA sequence or nucleotide tri-phosphate building block. During discussion of reaction mechanisms, one important issue to be discussed is about which group acted as reducing agent for Ag(I) reduction. The ATP molecule contains hydroxyl groups on its sugar part as shown in Fig. 1. It has been reported that molecules containing hydroxyl group could act as a reducing agent in NPs synthesis under UV-irradiation [38–42]. Different hydroxyl compounds like ascorbic acid [38], TX-100 [39], dendrimer [40], 2,7-DHN [41], and poly (vinyl) alcohol (PVA) [42] could act as a reducing agent in NPs synthesis in the presence of UV-irradiation. These compounds have hydroxyl group on their skeleton which undergoes hydroxylic cleavage to a hydroxyl radical in the presence of UV-irradiation. The UV light generated hydroxyl radicals that could act as a reducing agent for reduction of metal ions to metal (0). Our group reported earlier that hydroxylic compounds could reduce Au(III) [43], Pd(II) [44], Pt(IV) [45] and Rh(III) [42] ions to produce their corresponding NPs with different morphology. We also reported previously that DNA having hydroxyl groups in its sugar could act as a reducing agent in the synthesis of metal [31] and semi-conductor [2] nanowires. These hydroxyl groups probably acts as a reducing agent and are oxidized to ketones after the reduction. So here it is reasonable to assume that the hydroxyl radicals were formed during UV-irradiation of the solution mixture containing Ag ions and ATP promoted the reduction of Ag(I) to Ag(0). Once the nucleation of Ag(0) started to grow, it would involve in multiple steps and eventually generate Ag NPs in different sizes. In the first step of reduction of Ag(I) to Ag(0), Ag atoms were formed. The Ag atoms subsequently grew to form small Ag nuclei and finally the crystalline Ag particles. The ATP molecule having different groups were adsorbed onto the surface of these crystal particles and slowed down the growth rate of different crystal facets. Finally after 30 min of UV-irradiation, different sized Ag NPs were formed which in turn depended upon the concentrations of both Ag(I), ATP and UV-irradiation time. We assume that different parts of ATP have some specific roles in NPs synthesis (as shown in Fig. 1B). The three phosphate group and 'N' group assisted NP growth, the amine group helped for NP stabilization, and the hydroxyl group in the sugar part helps the radical generation. Similar types of results were shown earlier with GTP by Berti and Burley for the synthesis of inorganic NPs [46]. In our study, we have seen that smaller spheres were formed at a high concentration of both Ag(I) and ATP. At a high Ag(I) concentration once the nucleation started, a huge number of Ag nuclei were formed. Due to high concentration of ATP, the pre-formed Ag nuclei did

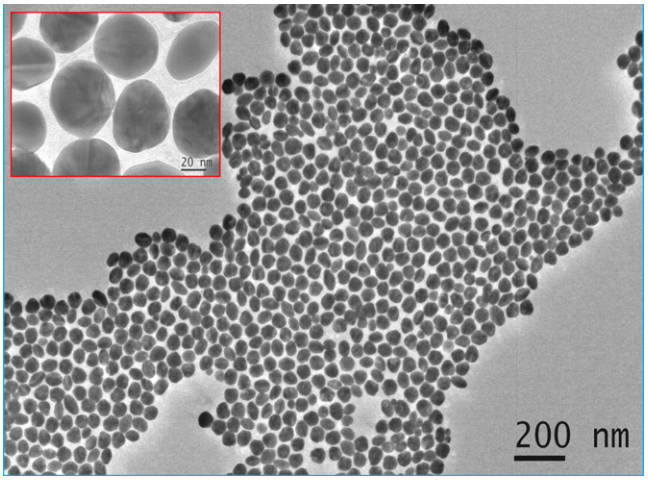

Fig. 7. Transmission electron microscopy (TEM) images of positively charged CTAB stabilized Ag NPs having average particles diameter ~45 ± 5 nm. Inset shows the corresponding higher magnified image.

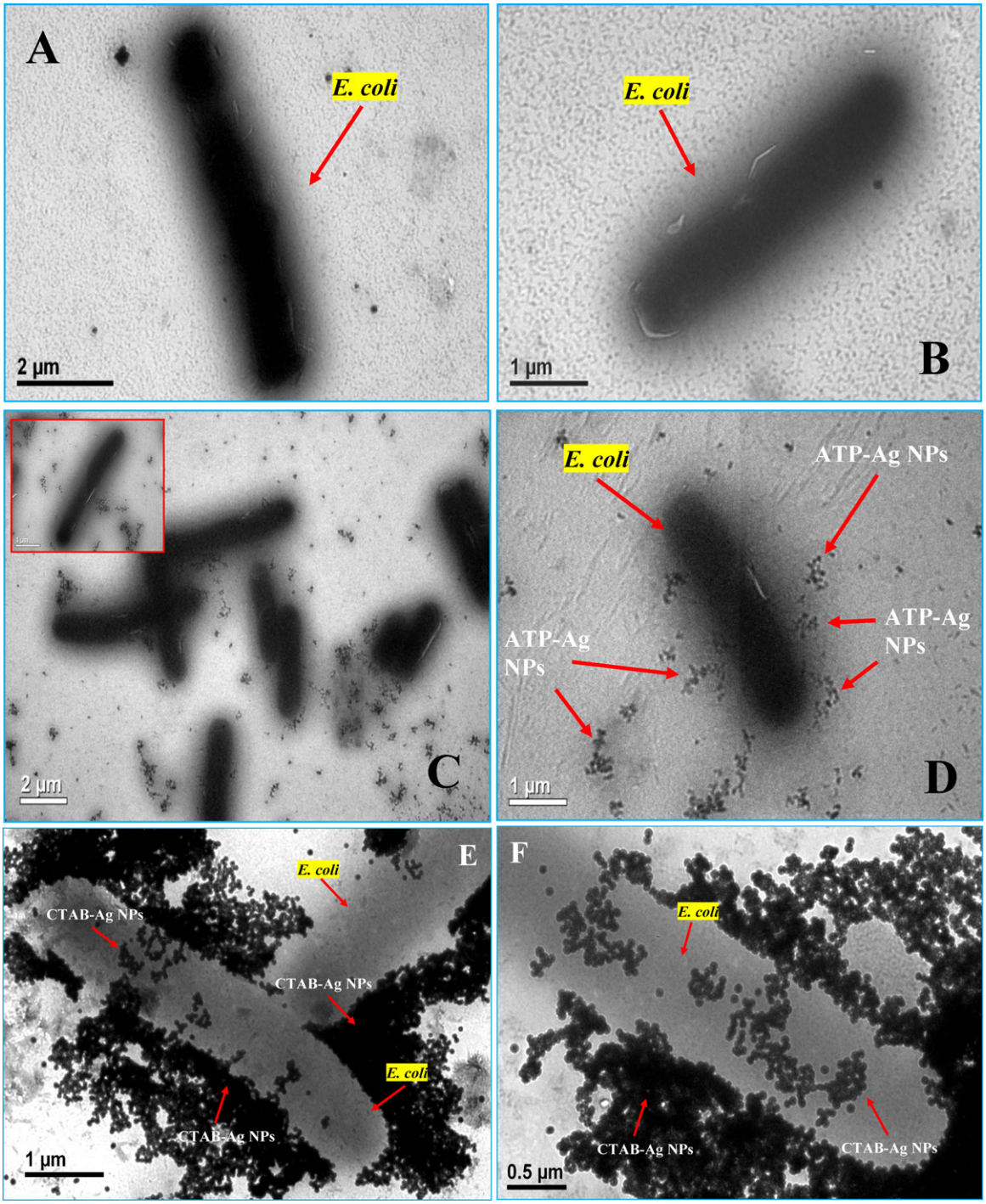

Fig. 8. Transmission electron microscopy (TEM) images of the bacteria *E. coli* with the Ag NPs at different reaction conditions. (A and B) Shows the image of only bacteria *E. coli* at different magnifications having average diameter is ~4 ± 1 μm. (C and D) Shows the low and high magnified TEM image of the bacteria after incubation with ATP–Ag NPs for 30 min. The inset of (C) shows the corresponding high magnified image. (E and F) Shows the low and high magnified TEM image of the *E. coli* with CTAB–Ag NPs after 30 min of incubation.

not get much free space to grow thus formed mall size Ag NPs. When the Ag(I) concentration was relatively low, lesser number of Ag nuclei were formed and received much space to grow and to form a bigger sized Ag NPs. The aggregated Ag nanostructures were observed both at a lower concentrations of Ag(I) and ATP. At lower concentration the interaction of the cationic part or the ATP with different crystal facets was slow and growth of the particles took place in all directions and produced big size aggregated particles. Once a particle was formed, they tried to bind with the nearest particles in order to lower the surface energy which was facilitate to low concentration of ATP. So the aggregated spherical Ag nanostructures were formed in the solution. It is well known that the formation of definite size and shape depends mostly on two factors, firth the faceting tendency of stabilizing agents and second the growth kinetics of Ag that is rate of supply of Ag(0) to the different crystallographic planes. The similar growth mechanism of the Ag particles formation was reported [16,21]. The present method of Ag NPs formation can find various important applications as ATP on its surface. They can act as a molecular spacer for SERS study or other biological applications. We also tested our study with other

nucleoside like ADP, AMP which results Ag particles but detailed study will be discussed in future. Taking the ATP stabilized Ag NPs and CTAB stabilized Ag NPs, we further study their interactions with bacteria *E. coli* as discussed below.

3.8. Interaction of Ag NPs with the bacterium E. coli

The interactions of Ag NPs against gram negative bacterium *E. coli* has been studied in details. In the study we used two types of Ag NPs, one is synthesized using ATP via the present method and another using previously reported method. The ATP stabilized Ag NPs are negatively charged whereas CTAB stabilized Ag NPs are positively charged. The bacterium *E. coli*, is one of the important food borne pathogens in the food industry. Recently, nano-sized particles are used widely as an antimicrobial agent [47]. Sondi and Salopek et al. studied the interaction of Ag NPs with *E. coli* and observed that majority of Ag NPs were located on the membrane of the cells [48]. Another study revealed that interaction of *E. coli* with nano sized Ag particles resulted in an immediate dissipation of the proton motive force and killing the cells [49]. The ATP stabilized Ag NPs that we used were 37 ± 5 nm in diameter where as the CTAB stabilized Ag NPs were 45 ± 5 nm in diameter. Fig. 7 shows the TEM image of CTAB stabilized positively charged Ag NPs and the inset shows the corresponding higher magnified image. From those images it is clear that the average diameter of the CTAB–Ag NPs was $\sim 45 \pm 5$ nm. Fig. 8 shows the TEM image of the bacteria with the Ag NPs. Fig. 8A and B shows the TEM image of bacteria *E. coli* at different magnification and different orientations. The average length of the bacteria was $\sim 4 \pm 1$ μm. The diameter of the bacteria could be changed by controlling the growth time during incubation at 37 °C. For two different types of NPs, we calculated the number of particles and added approximately the same number of particles during the incubation with bacteria such that we could compare their interactions. The number of particles or the surface area of the particles in solution was calculated based on the concentration of silver salt used to make the solution. This calculation technique was based on three points into consideration. Firstly, we assume that most of the particles in a particular solution were in same shape as confirmed from TEM images. Secondly, the density of bulk silver was the same as that of the NPs that had been confirmed by the similar crystal structure and bond lengths. Finally the yield of NPs was assumed to be 100%, i.e., that all the Ag salt is converted to Ag NPs. Fig. 8C and D shows the low and high magnified TEM images of the bacteria after incubation with ATP–Ag NPs for 30 min. From the image it is seen that some of the Ag NPs interact with the bacteria surface and some not. The inset of Fig. 8C shows the corresponding high magnified image. The interactions of ATP–Ag NPs with bacteria surface and un-interacted Ag NPs are clearly indicated with red arrows in Fig. 8D. (For interpretation of the references to color in this text, the reader is referred to the web version of this article.) Fig. 8E and F shows the TEM image of the *E. coli* with CTAB stabilized Ag NPs after 30 min of incubation. Fig. 8E is the low magnified image where as Fig. 8F is the high magnified image. From the two images it is clear that a high number of NPs are interacted on the bacteria surface compared to previous ones (Fig. 8C and D). The red arrows indicate the CTAB–Ag NPs on the bacteria surface like before. The interactions of the two differently charged Ag NPs with bacteria are most likely to be with the lipopolysaccharide component of the outer membrane surface of the *E. coli*. The gram negative bacterium surfaces are chemically different than the gram positive bacterium surface. The gram positive bacterium surface contains the teichoic acid group which has negatively charged phosphate group whereas gram negative bacterium surface mostly contains proteins, phospholipids and lipopolysaccharides (LPSs) [50,51]. The phospholipids and LPS in the outer membrane also contain negatively charged phosphate group. So the interaction or the depositions of NPs on the bacterium surface are different. When ATP–Ag NPs are mixed with the bacterium surface they repeal each other and the deposition is less (as shown in Fig. 8C and D). On the other hand, CTAB–Ag NPs are oppositely charged so they attracted and deposition is more on the bacterium surface (as shown in Fig. 8E and F) compared to ATP–Ag NPs. We found that a specific charge of the NPs is strongly affecting their deposition on the bacteria substrate. To further confirm the NPs deposition on the bacterium surface an EDS study was done as shown in Fig. 9A and B. Fig. 9A shows the EDS of only bacteria itself and 9B for the bacteria and Ag NPs conjugates. We checked with both ATP–Ag NPs and CTAB–Ag NPs for this study. Fig. 9B shows the additional Ag peak including the other as in Fig. 9A. This result confirms that Ag NPs deposited on bacteria cell wall and they interacted with the surface. So our present study give us an idea about how the different surface charge of NPs interact different ways with the microorganisms. Although at the point we are not fully clear whether the NPs are inserted inside the bacteria cell wall or not, further studies are required to investigate this. These will be reported in near future.

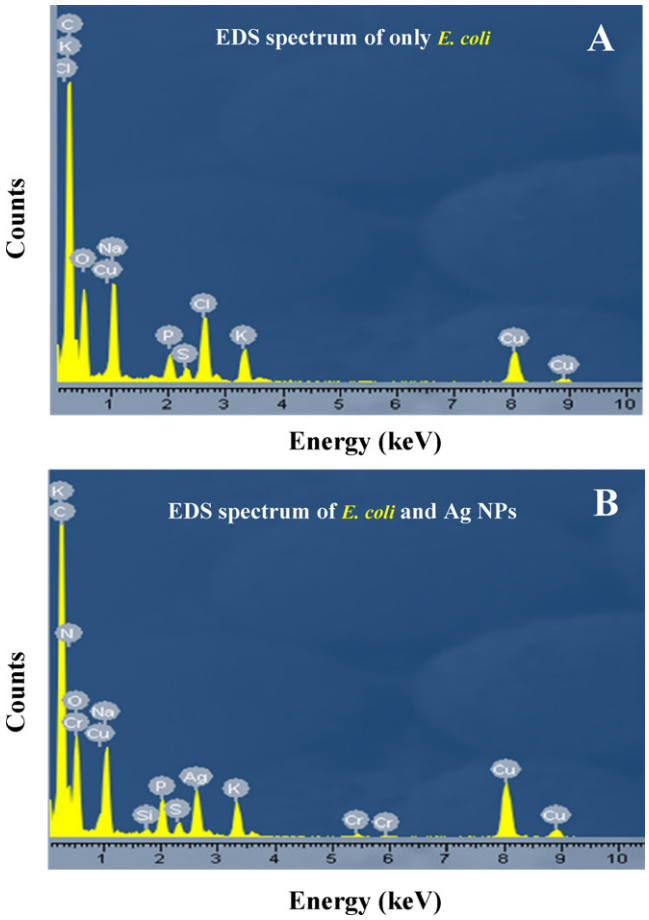

Fig. 9. Energy dispersive X-ray spectrum (EDS) of the bacteria itself (A) and bacteria and Ag NPs conjugates (B).

4. Conclusion

In the present research, we have demonstrated two new aspects. First, we were able to synthesize size-selective Ag NPs within 30 min of UV-irradiation in the presence of ATP. ATP served as a reducing agent during the synthesis as well as stabilizing agent after the formation of Ag particles. The synthesis was efficient, straight forward and did not need any harsh reduction conditions. The synthesized particles were stable for more than a month under ambient

conditions without indication of oxide formation. Second, we have studied the interactions of positively and negatively charged Ag NPs with bacterium *E. coli*. We observed that positively charged Ag NPs deposited better with the bacteria surface compared with the negatively charged. The present research could find new applications for a fast synthesis process of other nanomaterials as well as to understand the interactions of NPs with microorganisms.

Acknowledgements

This research was in part sponsored by the NSF-0506082; the Department of Mechanical Engineering, Texas A&M University; and the Texas Engineering Experiments Station. We wish to thank Yan Zhao for supplying bacteria samples from Biological Science Department in TAMU. Supports for TEM and EDS by Dr. Zhiping Luo at the Microscopy Imaging Center (MIC), Texas A&M University were greatly appreciated.

References

[1] A.P. Alivisatos, Science 271 (1996) 933–937.
[2] S. Kundu, H. Liang, Adv. Mater. 20 (2008) 826–831.
[3] M. Mandal, S. Kundu, T.K. Sau, S.M. Yusuf, T. Pal, Chem. Mater. 15 (2003) 3710–3715.
[4] H. Fang, Y. Wu, J. Zhao, J. Zhu, Nanotechnology 17 (2006) 3768–3774.
[5] B.T. Anto, S. Sivaramakrishnan, L.L. Chua, P.K.H. Ho, Adv. Funct. Mater. 20 (2010) 296–303.
[6] V. Wong, M.A. Ratner, J. Phys. Chem. B 110 (2006) 19243–19253.
[7] D. Lee, R.E. Cohen, M.F. Rubner, Langmuir 21 (2005) 9651–9659.
[8] M.J. Beier, T.W. Hansen, J.D. Grunwaldt, J. Catal. 266 (2009) 320–330.
[9] S. Nie, S.R. Emory, Science 275 (1997) 1102–1106.
[10] M. Prochazka, J. Stepanek, P.Y. Turpin, J. Bok, J. Phys. Chem. B 106 (2002) 1543–1549.
[11] G. Frens, Nature 241 (1972) 20–22.
[12] P.V. Silvert, R.H. Urbina, K.T. Elhsissen, J. Mater. Chem. 7 (1997) 293–299.
[13] J.L. Marignier, J. Belloni, M.O. Delcourt, J.P. Chevalier, Nature 317 (1985) 344–345.
[14] R.A. Salkar, P. Jeevanandam, S.T. Aruna, Y. Koltypin, A. Gedanken, J. Mater. Chem. 9 (1999) 1333–1335.
[15] T. Tsuji, T. Mizuki, S. Ozono, M. Tsuji, J. Photochem. Photobiol. A: Chem. 206 (2009) 134–139.
[16] S. Kundu, K. Wang, H. Liang, J. Phys. Chem. C 113 (2009) 134–141.
[17] F.K. Liu, P.W. Huang, T.C. Chu, F.H. Ko, Mater. Lett. 59 (2005) 940–944.
[18] Y. Tan, X. Dai, Y. Li, D. Zhu, J. Mater. Chem. 13 (2003) 1069–1075.
[19] S. Kundu, V. Maheshwari, S. Niu, R.F. Saraf, Nanotechnology 19 (2008) 65604–65609.
[20] S. Kundu, M. Mandal, S.K. Ghosh, T. Pal, J. Colloid Interface Sci. 272 (2004) 134–144.
[21] V.G. Pol, D.N. Srivastava, O. Palchik, V. Palchik, M.A. Slifkin, A.M. Weiss, A. Gedanken, Langmuir 18 (2002) 3352–3357.
[22] S. Behrens, A. Heyman, R. Maul, S. Essig, S. Steigerwald, A. Quintilla, W. Wenzel, J. Buerck, O. Dgany, O. Shoseyov, Adv. Mater. 21 (2009) 3515–3519.
[23] M.J. Kogan, I. Olmedo, L. Hosta, A.R. Guerrero, L.J. Cruz, F. Albericio, Nanomedicine 2 (2007) 287–306.
[24] B. Hu, S.-B. Wang, K. Wang, M. Zhang, S.-H. Yu, J. Phys. Chem. C 112 (2008) 11169–11174.
[25] G. Wei, H. Zhou, Z. Liu, Y. Song, L. Wang, L. Sun, Z. Li, J. Phys. Chem. B 109 (2005) 8738–8743.
[26] J. Zhang, Y. Liu, Y. Ke, H. Yan, Nano Lett. 6 (2006) 248–251.
[27] N. Seeman, Curr. Opin. Struct. Biol. 6 (1996) 519–526.
[28] M.C. SanMartin, C. Gruss, J.M. Carazo, J. Mol. Biol. 268 (1997) 15–20.
[29] N. Ma, C.J. Dooley, S.O. Kelley, J. Am. Chem. Soc. 128 (2006) 12598–12599.
[30] L.A. Gugliotti, D.L. Feldheim, B.E. Eaton, J. Am. Chem. Soc. 127 (2005) 17814–17818.
[31] S. Kundu, H. Liang, Langmuir 24 (2008) 9668–9674.
[32] H. Wei, Y. Wang, E. Wang, Nanotechnology 18 (2007) 175610–175615.
[33] T. Yonezawa, S. Ya, Onoue, N. Kimizuka, Langmuir 16 (2000) 5218–5220.
[34] Z.L. Wang, J. Phys. B: At. Mol. Opt. Phys. 104 (2000) 1153–1175.
[35] C. Weiping, Z. Huicai, L. Zhang, J. Appl. Phys. 83 (1998) 1705–1710.
[36] A. Kumar, S. Mital, J. Colloid Interface Sci. 240 (2001) 459–466.
[37] M. Green, R. Taylor, G. Wakefield, J. Mater. Chem. 13 (2003) 1859–1861.
[38] A. Pal, T. Pal, J. Raman Spectrosc. 30 (1999) 199–204.
[39] A. Pal, Talanta 46 (1998) 583–587.
[40] K. Esumi, A. Suzuki, N. Aihara, K. Usui, K. Torigoe, Langmuir 14 (1998) 3157–3159.
[41] S. Kundu, K. Wang, H. Liang, J. Phys. Chem. C 113 (2009) 18570–18577.
[42] S. Kundu, D. Huitink, K. Wang, H. Liang, J. Colloid Interface Sci. 344 (2010) 334–342.
[43] S. Kundu, L. Peng, H. Liang, Inorg. Chem. 47 (2008) 6344–6352.
[44] S. Kundu, K. Wang, D. Huitink, H. Liang, Langmuir 25 (2009) 10146–10152.
[45] S. Kundu, H. Liang, Langmuir 26 (2010) 6720–6727.
[46] L. Berti, G.A. Burley, Nat. Nanotechnol. 3 (2008) 81–87.
[47] M. Raffi, F. Hussain, T.M. Bhatti, J.I. Akhter, A. Hameed, M.M. Hasan, J. Mater. Sci. Technol. 24 (2008) 192–196.
[48] I. Sondi, B. Salopek-Sondi, J. Colloid Interface Sci. 275 (2004) 117–182.
[49] V.K. Sharma, R.A. Yngard, Y. Lin, Adv. Colloid Interface Sci. 145 (2009) 83–96.
[50] T.J. Beveridge, J. Bacteriol. 181 (1999) 4725–4733.
[51] T.J. Beveridge, Int. Rev. Cytol. 72 (1981) 229–317.